J Mater Sci (2014) 49:6674–6681
DOI 10.1007/s10853-014-8339-4

ULTRAFINEGRAINED MATERIALS

Improvement of strength and conductivity in Cu-alloys with the application of high pressure torsion and subsequent heat-treatments

D. V. Shangina · J. Gubicza · E. Dodony · N. R. Bochvar · P. B. Straumal · N. Yu. Tabachkova · S. V. Dobatkin

Received: 14 March 2014 / Accepted: 19 May 2014 / Published online: 3 June 2014

Abstract Quenched and slowly cooled (annealed) Cu–0.7 %Cr, Cu–0.9 %Hf, and Cu–0.7 %Cr–0.9 %Hf alloys were processed by high pressure torsion (HPT). The microstructures of the alloys were studied immediately after HPT and subsequent annealing. It has been shown that the microhardness and the thermal stability of the severely deformed microstructure increase, while the average grain size decreases in the order of Cu–0.7 %Cr, Cu–0.9 %Hf, and Cu–0.7 %Cr–0.9 %Hf alloys. The microhardness in all alloys is higher after quenching and HPT, than after annealing and HPT. The largest dislocation density is achieved by quenching and HPT in Hf-containing samples. Cu_5Hf phase precipitations in Hf-containing alloys are more effective in retarding grain growth in comparison with Cr particles and lead to additional hardening during aging. It has been demonstrated that HPT-processing with subsequent heat-treatment might yield the combination of large hardness and high electrical conductivity in Cu alloys.

D. V. Shangina · N. R. Bochvar · P. B. Straumal · S. V. Dobatkin
A.A.Baikov Institute of Metallurgy and Materials Science, Russian Academy of Sciences, Leninskiy prospect 49, 119991 Moscow, Russia
e-mail: Bochvar@imet.ac.ru

P. B. Straumal
e-mail: Straumal.peter@yandex.ru

S. V. Dobatkin
e-mail: Dobatkin@hotmail.ru

D. V. Shangina (✉) · P. B. Straumal · N. Yu. Tabachkova · S. V. Dobatkin
Laboratory of Hybrid Nanostructured Materials, National Science and Technology University "MISIS", Leninskiy prospect 4, 119049 Moscow, Russia
e-mail: shanginadaria@mail.ru

N. Yu. Tabachkova
e-mail: Ntabachkova@gmail.com

J. Gubicza · E. Dodony
Department of Materials Physics, Eotvos Lorand University, Pázmány Péter sétány 1/A, Budapest 1117, Hungary
e-mail: Jeno.gubicza@ttk.elte.hu

E. Dodony
e-mail: Dodonye@gmail.com

Introduction

The application of severe plastic deformation (SPD) usually results in significant grain refinement in metals and alloys [1, 2]. The ultrafine grained (UFG) microstructures exhibit improved mechanical properties such as high strength, good fatigue durability, wear resistance, etc. [2–4]. However, the high densities of lattice defects (e.g., dislocations and grain boundaries) yield deterioration of other functional properties, such as ductility, workability, and electric conductivity. However, it has been shown recently that the application of SPD-processing and a subsequent moderate heat-treatment might lead to a combination of high strength and good ductility. The improvement of mechanical properties in copper alloys, such as Cu–Cr, Cu–Zr, Cu–Hf, Cu–Cr–Zr, and Cu–Cr–Hf, is also important from the point of view of their application in the electrotechnical industry. It has been shown that SPD-processing using either equal-channel angular pressing (ECAP) [5–15] or high pressure torsion (HPT) [16–21] yielded considerable strength increment due to the grain refinement in these alloys. However, the high defect density introduced in the material by SPD increases the electrical resistance, thereby reducing the applicability. Therefore, it is an open question whether it is possible to

increase the high strength in these copper alloys while maintaining the good conductivity. Moderate heat-treatments after SPD-processing may improve significantly the conductivity with a slight reduction in strength. In this paper, the influence of heat-treatments after HPT-processing on the microstructure, strength, and electrical conductivity in precipitation-hardenable Cu–Cr, Cu–Hf, and Cu–Cr–Hf copper alloys is studied.

Materials and methods

The experiments were conducted on Cu–0.7 %Cr, Cu–0.9 %Hf and Cu–0.7 %Cr–0.9 %Hf alloys (in wt%). The alloys were melted in an arc furnace under purified argon atmosphere using M0b grade Cu (99.97 %), ERKh grade Cr (99.96 %), and Hf (99.8 %) charge materials. The as-cast Cu–0.7 %Cr and the Hf-containing alloys were subjected to homogenization heat-treatments for 1 h at 1000 and 900 °C, respectively. Then, the alloys were cooled down to room temperature at two different routes: water quenching or slow cooling with furnace. Hereafter, the samples cooled by the former and the latter processes are referred to as quenched and annealed initial specimens, respectively.

The cooled rods with a diameter of 10 mm and a length of 300 mm were cut to samples with a thickness of 0.3 mm and subjected to HPT in a Bridgman anvil at a speed of 1 rev/min at room temperature under a pressure of 4 GPa to a maximum true strain of $\sim$4.8 (five revolutions). The deformation was performed in a "groove" with the depth of 0.2 mm. The microhardness and the electrical conductivity were measured on the samples in the initial state and after HPT. The microhardness was measured using a 402 MVD Instron Wolpert Wilson Instruments tester with a load of 50 g and a holding time of 10 s. The hardness measurements were carried out at a distance of 2.5 mm from the sample center (mid-radius). The resistivity was measured using a BSZ-010-2 microhmmeter on flat samples with $0.3 \times 6 \times 10$ mm in size. The resistivity was calculated and transformed into electrical conductivity according to International Annealed Copper Standards (IACS). The microstructure was observed using JEM-2100 transmission electron microscope. Thin foils for electron microscopy were prepared by ion polishing with a GATAN 600 unit. The evolution of the microstructure, the hardness, and the conductivity were also studied during heat-treatments after HPT. The samples were heat-treated at temperatures ranging from 50 to 550 °C with a step of 50 °C and with a holding time of 1 h at each temperature.

The microstructure of the Cu matrix in selected specimens was studied by X-ray line profile analysis. The X-ray line profiles were measured by a high-resolution rotating anode diffractometer (Nonius, FR591) with CuKα_1 radiation (wavelength: $\lambda = 0.15406$ nm). The line profiles were evaluated by Convolutional Multiple Whole Profile (CMWP) fitting method [4, 22, 23]. In this procedure, the diffraction pattern is fitted by the sum of a background spline and the convolution of the instrumental pattern and the theoretical line profiles related to the crystallite size, dislocations, and twin faults. Because of the UFG microstructure of the studied samples, the physical broadening of the profiles was much larger than the instrumental broadening, therefore instrumental correction was not applied in the evaluation. The theoretical profile functions used in this fitting procedure are calculated on the basis of a model of the microstructure, where the crystallites have spherical shape and log-normal size distribution. As an example, the fitting for the sample Cu–0.7 %Cr–0.9 %Hf after annealing and HPT is shown in Fig. 1. The peaks of the secondary phases were incorporated in the background during fitting. The following parameters of the microstructure were determined from CMWP-fitting procedure: the area weigthed mean crystallite size ($<x>_{area}$), the dislocation density (ρ), the parameter q describing the edge/screw character of dislocations, the dislocation arrangement parameter (M), and the twin boundary probability (β). The twin-boundary probability is defined as the fraction of twin boundaries among the {111} lattice planes. The value of $<x>_{area}$ is calculated as $<x>_{area} = m\exp(2.5\sigma^2)$, where m is the median and σ is the variance of the crystallite size distribution.

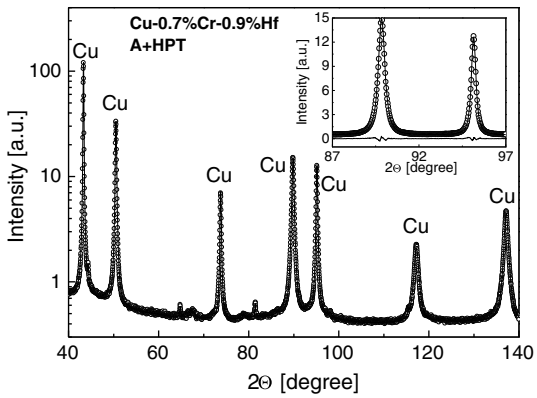

Fig. 1 The CMWP fitting for the sample Cu–0.7 %Cr–0.9 %Hf after annealing and HPT. The *open circles* and the *solid line* represent the measured data and the *fitted curves*, respectively

Results and discussion

Initial state

All the investigated alloys are precipitation hardenable, and the initial structure of the alloys is in accordance with the phase-diagrams given in Fig. 2. After annealing, the alloys

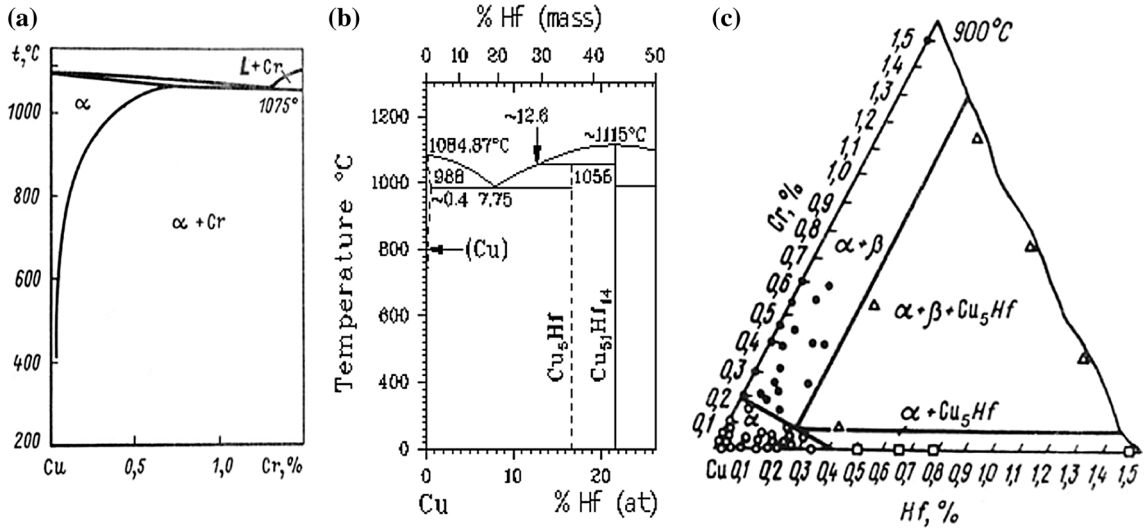

Fig. 2 Phase states diagrams **a** Cu-rich region in binary Cu–Cr system, **b** Cu-rich region in binary Cu–Hf system, **c** The isothermal section of the ternary system Cu–Cr–Hf at 900 °C

structure consists of Cu-based solid solution grains (with an average size of ~200 μm in Cu–0.7 %Cr alloy and ~150 μm in Cu–0.9 %Hf and Cu–0.7 %Cr–0.9 %Hf alloys) and particles of Cr-based solid solution (with an average size of about 1.5 μm in Cu–0.7 %Cr alloy and Cu_5Hf compound with ~3 μm in size in Cu–0.9 %Hf alloy). In ternary Cu–0.7 %Cr–0.9 %Hf alloy, both types of particles are present. In the quenched samples, Cu_5Hf phase was not observed (i.e., the Hf was in solid solution), while in the Cr-containing alloys particles of Cr were detected as the chromium content was above the solubility limit in copper even at the temperature of heat-treatment before HPT (900–1000 °C, see Fig. 2). The fraction of Cr phase in the quenched alloys was lower than in the annealed samples.

TEM analysis of structure, microhardness and electrical conductivity of Cu alloys after HPT and subsequent heating

Cu–0.7 %Cr alloy

Figure 3a and b presents the dependences of microhardness and electrical conductivity on the heating temperatures after HPT for the Cu–0.7 %Cr alloy. HPT leads to significant hardening in both annealed and quenched alloys due to the grain refinement and the very high dislocation density (see later). The microhardness and the conductivity of the quenched sample after HPT are slightly higher and considerably lower, respectively, than the values determined for the annealed and HPT-processed specimen, which can be explained by the higher solute Cr content. The hardness decreased while the conductivity increased above 250–300 °C due to the annihilation of lattice defects and the decomposition of the supersaturated Cu–Cr alloy. The initial quenching before HPT raises the starting temperature of hardness reduction from 250 to 300 °C due to the pinning effect of Cr-alloying atoms on lattice defects (e.g., dislocations). The increase of the electrical conductivity during heating at the temperatures above 250 °C is mainly caused by the decomposition of supersaturated solid solution into Cu matrix and disperse chromium precipitations. The increase in conductivity was also observed in the annealed sample after HPT, but the rate of change was less in this case.

In a previous work of the present authors, the influence of a preliminary heat treatment on properties of a Cu–0.7 %Cr alloy after HPT [20] was also studied. Quenching in water from temperature 900 °C and annealing at a temperature of 600 °C were applied. Comparing the results obtained in the previous and the present studies, it is revealed that the increase in temperature of quenching from 900 to 1000 °C did not lead to the change in microhardness after HPT. However, the thermal stability of the UFG structure increased when higher temperature was applied before quenching, due to the larger concentration of Cr in solid solution. For Cu–0.7 %Cr alloy quenched from 1000 and 900 °C before HPT, the reduction of hardness started at 300 and 250 °C, respectively. It should be noted that the increase of temperature before quenching also leads to an higher increment in hardness in the course of subsequent aging without deformation: after quenching from 900 °C and subsequent aging, the microhardness increased by 200 MPa, while after quenching from 1000 °C and aging this hardness increment was 500 MPa (see Fig. 3a). The increase in temperature of annealing from 600 to 1000 °C

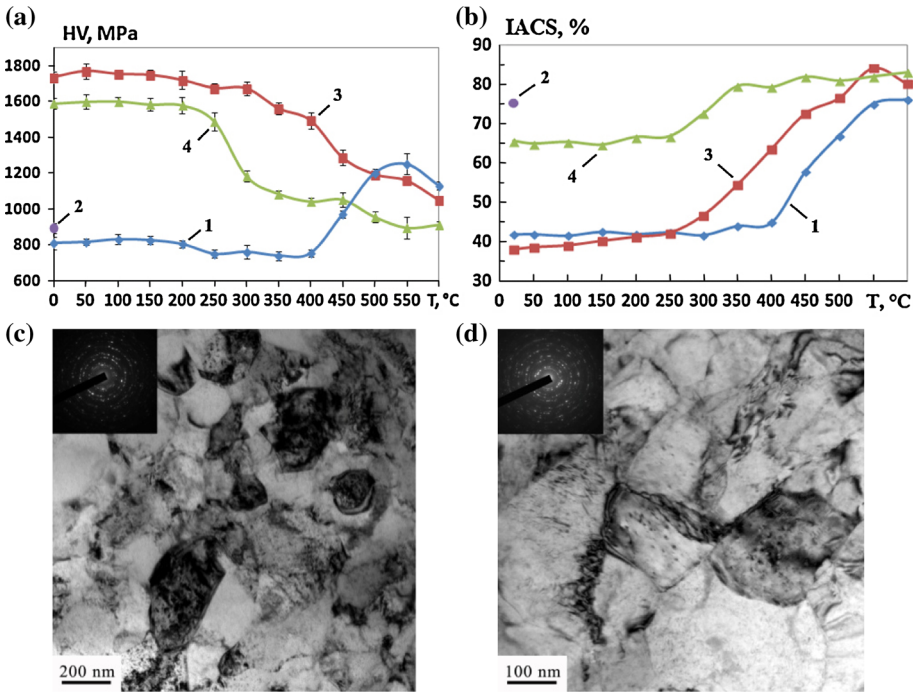

Fig. 3 Temperature dependences of (**a**) microhardness and (**b**) electrical conductivity (% of IACS) and structure of Cu–0.7 %Cr alloy (**c**) after quenching and HPT, (**d**) after quenching, HPT and aging at 250 °C. Treatments: 1-Water quenching from 1000 °C (1 h); 2-Annealing at 1000 °C for 1 h; 3-Water quenching from 1000 °C (1 h) + HPT; 4-Annealing at 1000 °C for 1 h + HPT

also leads to increase in thermal stability of the alloy after HPT. The initial temperature of hardness reduction increased from 100 to 250 °C.

After HPT, the Cu–0.7 %Cr alloys have nearly the same grain size (200–220 nm), irrespectively of the initial states (annealed or quenched). For example, Cu–0.7 %Cr alloy after quenching and HPT has the average grain size of 209 nm (see Fig. 3c). Electron microscopic analysis did not show new disperse particles that could be formed during HPT. In the course of the following heating up to 250 °C, when the hardness remains at the initial level, the average grain size becomes slightly larger (245 nm), the fraction of high-angle grain boundaries increases, the grain boundaries become more equilibrium and new Cr-phase particles are precipitated (see Fig. 3d). Most probably, the Cr-phase particles formed during aging slow down the matrix grain growth during heating. However, chromium particles are not able to significantly restrict the recrystallization processes; therefore at the end of the decomposition of solid solution, where the alloy has a high electrical conductivity, considerable softening can be observed. It should be noted that HPT accelerates the decomposition as the considerable increment in conductivity starts at lower temperature for the quenched state after HPT than for the quenched undeformed material (see Fig. 3b).

Cu–0.9 %Hf alloy

The microhardness of the Cu–0.9 %Hf alloy after quenching and HPT is 200 MPa higher than in Cu–0.7 %Cr alloy (see Fig. 4a), mostly due to the smaller average grain size (155 nm) (see Fig. 4c). Unlike the previous alloy, the preliminary heat treatment does not affect significantly the thermal stability after HPT but strongly influences the strength. The microhardness values in the quenched Cu–0.9 %Hf alloy after HPT are higher than in the annealed state and the difference increases during aging, due to decomposition of supersaturated solid solution resulting in the formation of Cu_5Hf particles (with a size about 20 nm) (see Fig. 4d). The decomposition of the alloy is confirmed by the considerable increase of conductivity during heating after quenching and HPT (see Fig. 4b). This indicates that the particles of the intermetallic compound Cu_5Hf are more effective in hardening and retarding grain growth in bronzes after HPT and subsequent heating than the Cr particles. After heating for1 h at 450 °C, the average grain size of the Cu–0.9 %Hf alloy after quenching and HPT slightly increased to 189 nm. Thus, the good combination of microhardness (2400 MPa) and electrical conductivity (71 %IACS) can be reached by aging at the temperature of 450 °C after HPT of the quenched initial state.

Cu–0.7 %Cr–0.9 %Hf alloy

The hardness of the Cu–0.7 %Cr–0.9 %Hf alloys after quenching and HPT is the highest among the three alloys (Fig. 5a) which can be attributed to the effects of the relatively large alloying element concentration and the very small average grain size in the matrix (108 nm, Fig. 5c).

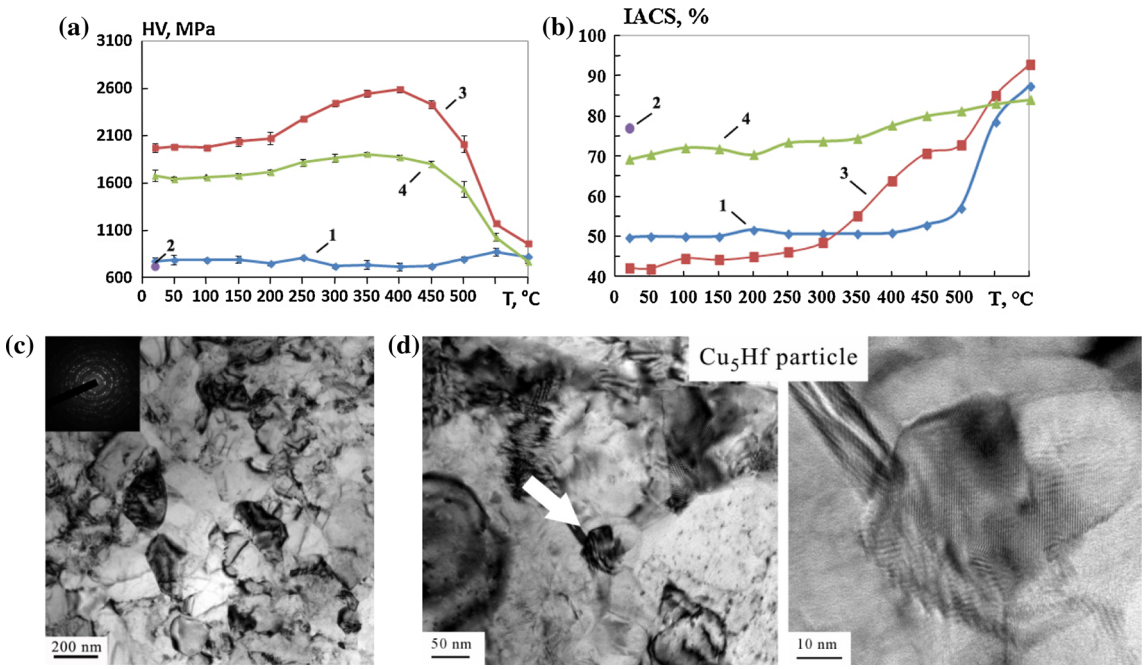

Fig. 4 Temperature dependences of (**a**) microhardness and (**b**) electrical conductivity (% of IACS) and structure of Cu–0.9 %Hf alloy (**c**) after quenching and HPT, (**d**) after quenching, HPT and aging at 450 °C. Treatments: 1-Water quenching from 900 °C (1 h); 2-Annealing at 900 °C for 1 h; 3-Water quenching from 900 °C (1 h) + HPT; 4-Annealing at 900 °C for 1 h + HPT

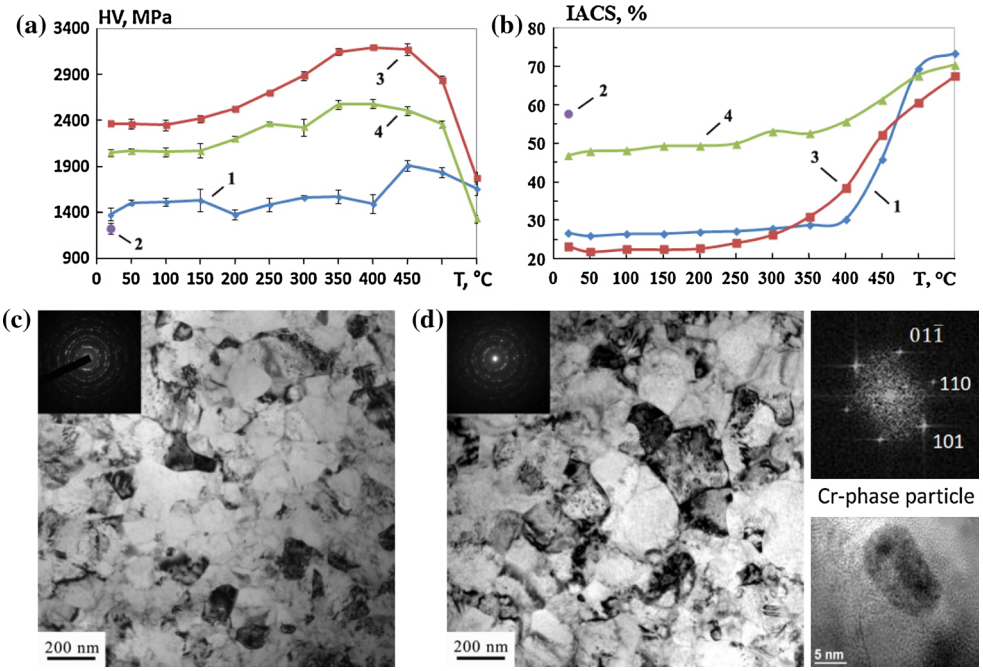

Fig. 5 Temperature dependences of (**a**) microhardness and (**b**) electrical conductivity (% of IACS) and structure of Cu–0.7 %Cr–0.9 %Hf alloy (**c**)after quenching and HPT, (**d**) after quenching, HPT and aging at 500 °C. Treatments: 1-Water quenching from 900 °C (1 h); 2-Annealing at 900 °C for 1 h; 3-Water quenching from 900 °C + HPT (1 h); 4-Annealing at 900 °C for 1 h + HPT

The hardening caused by aging can be explained by precipitation of both Cr and Cu_5Hf particles. A Cr-phase particle with the size of 10–15 nm is shown in Fig. 5d.

The influence of the initial state on the hardness and the thermal stability after HPT in the ternary alloy is similar to the case of the Cu–0.9 %Hf alloy, but the difference between the behaviors of the quenched and annealed materials is higher (Fig. 5a, b). Complex alloying with Cr and Hf rises the microhardness after quenching and HPT up to 2400 MPa, but in this case the electrical conductivity is quite low (23 % of IACS). Subsequent heating causes further hardening of the alloy up to 3200 MPa, but the best combination of microhardness (2800 MPa) and electrical conductivity (61 % of IACS) is received after heating at

500 °C (Fig. 5a, b). The thermal stability of this alloy is the best among all the investigated alloys, and the hardness starts to decrease only above 500 °C. After 1 h holding at this temperature, the average grain size of the Cu–0.7 %Cr–0.9 %Hf alloy after quenching and HPT slightly increased to 131 nm (Fig. 5d). In this case, we also observed that HPT accelerates the decomposition kinetics, since the conductivity starts to increase at lower temperature for the quenched and HPT-processed material than in the case of the quenched sample.

Thus, the strength and thermal stability of the low-alloyed bronzes processed by HPT increase in the following order: Cu–0.7 %Cr, Cu–0.9 %Hf, and Cu–0.7 %Cr–0.9 %Hf. The possibility of simultaneous improvement of strength and electrical conductivity in UFG copper alloys was demonstrated. HPT and subsequent heating leads to the increase of strength, while the electrical resistivity value becomes lower than in the initial state due to the decomposition of supersaturated solid solution. Besides the phase composition, the lattice defect structure also influences both the hardness and the resistivity, therefore the dislocation structure was additionally investigated in the next section.

X-ray line profile analysis of Cu alloys after HPT and subsequent heating

The HPT-processed Cu-alloys and the specimens heat-treated at the temperature corresponding to the beginning of softening were studied by X-ray line profile analysis. These temperatures are 250, 450, and 500 °C for Cu–0.7 %Cr, Cu–0.9 %Hf, and Cu–0.7 %Cr–0.9 %Hf alloys, respectively. The parameters of the microstructure for the studied samples are listed in Table 1. For $\frac{1}{2}\langle 110\rangle\{111\}$ slip system in Cu, the values of parameter q describing the edge/screw character of dislocations are 1.67 and 2.33, respectively. For all the studied samples, the experimental value of q was between 2.0 and 2.2, indicating that the character of dislocations is rather screw type. Table 1 reveals that in the quenched specimens containing Hf, the dislocation density after HPT is higher by about 50 % than in the annealed samples. Simultaneously, the crystallite size is slightly smaller in the quenched and HPT-processed samples, as compared to the specimens annealed and deformed by HPT. The effect of quenching on the X-ray diffraction peak broadening is illustrated in Fig. 6 where the full width at half maximum (FWHM) is plotted as a function of the length of the diffraction vector (g) for Cu–0.7 %Cr–0.9 %Hf alloy after quenching+HPT and annealing+HPT (Williamson-Hall plot). For all reflections, the FWHM of the quenched sample is much larger than for the annealed specimen, in accordance with the smaller crystallite size and the higher dislocation density in the former material. This means that in the Hf-containing specimens, the larger dislocation density has a contribution to the larger hardness of the quenched materials compared to the annealed samples after HPT-processing. However, in the samples containing only Cu and Cr, the effect of annealing or quenching on the defect structure is marginal. It is noted that these dislocation densities are very close to the value achieved by HPT in pure Cu (about 40×10^{14} m^{-2}) [24]. The twin boundary probability for all the samples was under the detection limit which is about 0.1 % corresponding to the twin boundary spacing of about 200 nm. This observation is in accordance with the TEM images. It should be noted that in the quenched and HPT-processed state, the dislocation density in the Hf-containing alloys was larger than in the alloy contains only Cr as alloying element. This difference contributes to the larger hardness of the Hf-containing samples after HPT.

The dislocation density decreased by about 40–50 % in the Hf-containing samples due to the heat-treatment after HPT. The dislocation arrangement parameter, M, decreased during heat-treatment, indicating the arrangement of

Table 1 The parameters of the microstructure obtained by X-ray line profile analysis: the area-weigthed mean crystallite size ($\langle x\rangle_{area}$), the dislocation density (ρ), the dislocation arrangement parameter (M), and the twin boundary probability (β)

Alloy/state	$\langle x\rangle_{area}$ [nm]	ρ [10^{14} m^{-2}]	M	β [%]
Cu–0.7 %Cr, Q+HPT	61 ± 6	41 ± 4	1.3 ± 0.1	0 ± 0.1
Cu–0.7 %Cr, A+HPT	64 ± 6	35 ± 4	1.3 ± 0.1	0 ± 0.1
Cu–0.7 %Cr, Q+HPT+H250	69 ± 7	42 ± 4	0.9 ± 0.1	0.1 ± 0.1
Cu–0.7 %Cr, A+HPT+H250	119 ± 13	20 ± 3	0.5 ± 0.1	0.3 ± 0.1
Cu–0.9 %Hf, Q+HPT	50 ± 5	64 ± 7	1.3 ± 0.1	0 ± 0.1
Cu–0.9 %Hf, A+HPT	61 ± 5	41 ± 4	1.3 ± 0.1	0 ± 0.1
Cu–0.9 %Hf, Q+HPT+H450	68 ± 6	39 ± 4	1.0 ± 0.1	0 ± 0.1
Cu–0.9 %Hf, A+HPT+H450	110 ± 10	26 ± 3	0.7 ± 0.1	0.2 ± 0.1
Cu–0.7 %Cr–0.9 %Hf, Q+HPT	47 ± 5	68 ± 7	1.3 ± 0.1	0 ± 0.1
Cu–0.7 %Cr–0.9 %Hf, A+HPT	60 ± 6	43 ± 4	1.3 ± 0.1	0.1 ± 0.1
Cu–0.7 %Cr–0.9 %Hf, Q+HPT+H500	90 ± 8	30 ± 3	0.4 ± 0.1	0.3 ± 0.1
Cu–0.7 %Cr–0.9 %Hf, A+HPT+H500	110 ± 12	19 ± 2	0.8 ± 0.1	0.2 ± 0.1

In the description of the sample state, the following notations are used: Q quenched, A annealed, H heat-treated (the value after H indicates the temperature in C°)

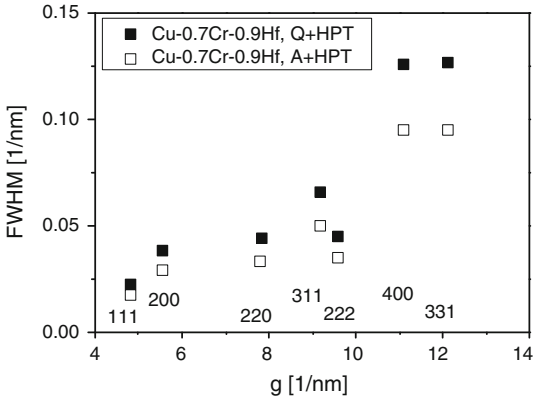

Fig. 6 Williamson-Hall plot for the samples "Cu–0.7 %Cr–0.9 %Hf, Q+HPT" and "Cu–0.7 %Cr–0.9 %Hf, A+HPT." *FWHM* full width at half maximum, *g* length of the diffraction vector

dislocations into low energy configurations in which the screening of the strain fields of dislocations is stronger than immediately after HPT (e.g., arrangement into dislocation dipoles). The twin boundary probability slightly increased due to heat-treatments which can be attributed to the formation of annealing twins. Additonally, the crystallite size increased by 40–90 %. These changes in the defect structure indicate a partial recovery of the HPT-processed microstructure. Despite the annihilation of dislocations, the hardness increases during the heat-treatments at 400–450 °C for Cu–0.9 %Hf and Cu–0.7 %Cr–0.9 %Hf alloys. Therefore, the increase of the hardness in the Hf-containing samples heat-treated at 400–450 °C can be attributed solely to the decomposition of solid solutions.

The crystallite size determined by X-ray line profile analysis was smaller than the grain size obtained by TEM for all the studied samples by a factor of 2–4. This observation can be explained by the fact that the crystallite size usually corresponds to the subgrain size in severely deformed microstructures. Therefore, there is no correlation between the crystallite and grain sizes, but rather they complementary describe the hierarchical nature of the microstructures obtained by SPD.

The present study revealed that quenching as a preliminary heat treatment is more effective than annealing for obtaining low-alloyed bronzes with high strength and good electrical conductivity. After HPT-processing of the quenched materials, the dislocation density was larger than for the annealed and HPT-processed states due to the stronger pinning effect of the higher solute atom concentration of Cr and Hf on dislocations in the quenched specimens. Both the higher dislocation density and the larger solute concentration in the quenched and HPT-processed materials yielded higher hardness and lower conductivity, as compared to the initially annealed materials. During subsequent heat-treatments, fine and well-dispersed precipitates were formed in the quenched samples, which resulted in a further increment in hardness, despite the decrease of the dislocation density. Simultaneosly, the conductivity was improved due to the decrease of solute content.

Conclusions

1. HPT leads to a significant strengthening of low-alloyed bronzes mainly due to the formation of UFG microstructure with a grain size of 209, 155, and 108 nm for Cu–0.7 %Cr, Cu–0.9 %Hf, and Cu–0.7 %Cr–0.9 %Hf alloys, respectively. The highest microhardness after HPT was obtained in the Cu–0.7 %Cr–0.9 %Hf alloy (2400 MPa).
2. HPT accelerates the supersaturated solid solution decomposition. Cu_5Hf phase precipitates are more effective for grain growth restriction in comparison with Cr particles and leads to additional hardening during aging. In Cu–0.7 %Cr–0.9 %Hf alloy, the microhardness reaches 3200 MPa due to Cu_5Hf phase precipitation during heat-treatment.
3. X-ray line profile analysis reveals that in the Hf-containing alloys the dislocation density is higher for the initially quenched and HPT-processed material than for the initially annealed and HPT-processed state. Therefore, the larger dislocation density contributes to the higher hardness for the former material. However, in the samples heat-treated at 400–450 °C, the dislocation density decreases, therefore the hardness increment during aging can be attributed solely to the decomposition of solid solutions, i.e., the formation of the secondary phase particles.
4. Application of SPD and subsequent heat-treatment in the studied Cu-alloys yields favorable combination of high strength and good conductivity.

Acknowledgements The work was supported by the Russian Foundation for Basic Research (Project13-08-00102), ERA.NetRUS (ProjectSTP-219), the Ministry of Education and Science of the Russian Federation (Project No.14.A12.31.0001) and the Hungarian Scientific Research Fund, OTKA, Grant No. K-109021.

References

1. Lowe TC, Valiev RZ (2000) Investigations and applications of severe plastic deformation. Kluwer Academic Publishing, Dordrecht
2. Zehetbauer MJ, Zhu YT (eds) (2009) Bulk nanostructured materials. Wiley, Weinheim
3. Valiev RZ, Zhilyaev AP, Langdon TG (2014) Bulk nanostructured materials: fundamentals and applications. Wiley, Hoboken, New Jersey

4. Sitarama Raju K, Subramanya Sarma V, Kauffmann A, Hegedus Z, Gubicza J, Peterlechner M, Freudenberger J, Wilde G (2013) High strength and ductile ultrafine-grained Cu–Ag alloy through bimodal grain size, dislocation density and solute distribution. Acta Mater. 61:228–238
5. Vinogradov A, Patlan V, Suzuki Y, Kitagawa K, Kopylov VI (2002) Structure and properties of ultra-fine grain Cu–Cr–Zr alloy produced by equal-channel angular pressing. Acta Mater. 50:1639–1651
6. Vinogradov A, Ishida T, Kitagawa K, Kopylov VI (2005) Effect of strain path on structure and mechanical behavior of ultra-fine grain Cu–Cr alloy produced by equal-channel angular pressing. Acta Mater. 53:2181–2192
7. Amouyal Y, Divinski SV, Estrin Y, Rabkin E (2007) Short-circuit diffusion in an ultrafine-grained copper–zirconium alloy produced by equal channel angular pressing. Acta Mater. 55:5968–5979
8. Kužel R, Cherkaska V, Matěj Z, Janeček M, Čížek J, Dopita M, Kristallogr Z (2008) Structural studies of submicrocrystalline copper and copper composites by different methods. Hausz fur Krist Suppl. 27:73–80
9. Wang QJ, Xu CZ, Zheng MS, Zhu JW, Du ZZ (2008) Fatigue crack initiation life prediction of ultra-fine grain chromium–bronze prepared by equal-channel angular pressing. Mater Sci Eng A. 496:434–438
10. Dopita M, Janeček M, Rafaja D, Uhlíř J, Matěj Z, Kužel R (2009) EBSD investigation of the grain boundary distributions in ultrarine-grained Cu and Cu-Zr polycrystals prepared by equal-channel angular pressing. Int J Mater Res. 100(6):785–789
11. Janeček M, Čížek J, Dopita M, Král R, Srba O (2008) Mechanical properties and microstructure development of ultrafine-grained Cu processed by ECAP. Mater Sci. Forum 584–586:440–445
12. Kužel R, Janeček M, Matěj Z, Čížek J, Dopita M, Srba O (2009) Microstructure of equal-channel angular pressed Cu and Cu-Zr samples studied by different methods. Metall Mater Trans A. 41(5):1174–1190
13. Valdes Leyn K, Munoz-Morris MA, Morris DG (2012) Optimisation of strength and ductility of Cu–Cr–Zr by combining severe plastic deformation and precipitation. Mater Sci Eng A. 536:181–189
14. Wongsa-Ngam J, Kawasaki M, Langdon TG (2012) The development of hardness homogeneity in a Cu–Zr alloy processed by equal-channel angular pressing. Mater Sci Eng A. 556:526–532
15. Jayakumara PK, Balasubramaniana K, Rabindranath Tagoreb G (2012) Recrystallisation and bonding behaviour of ultra fine grained copper and Cu–Cr–Zr alloy using ECAP. Mater Sci Eng A. 538:7–13
16. Dopita M, Janeček M, Kužel R, Seifert HJ, Dobatkin S (2010) Microstructure evolution of CuZr polycrystals processed by high-pressure torsion. J Mater Sci. 45:4631–4644. doi:10.1007/s10853-010-4643-9
17. Wongsa-Ngam J, Kawasaki M, Zhao Y, Langdon TG (2011) Microstructural evolution and mechanical properties of a Cu–Zr alloy processed by high-pressure torsion. Mater Sci Eng A. 528(25–26):7715–7722
18. Shangina DV, Bochvar NR, Dobatkin SV (2011) Structure and properties of ultrafine-grained Cu–Cr alloys after high pressure torsion. Mater Sci Forum. 667–669:301–306
19. Wongsa-Ngam J, Kawasaki M, Langdon TG (2012) Achieving homogeneity in a Cu–Zr alloy processed by high-pressure torsion. J Mater Sci. 47(22):7782–7788. doi:10.1007/s10853-012-6587-8
20. Shangina DV, Bochvar NR, Dobatkin SV (2012) The effect of alloying with hafnium on the thermal stability of chromium bronze after severe plastic deformation. J Mater Sci. 47(22):7764–7769. doi:10.1007/s10853-012-6525-9
21. Dobatkin SV, Shangina DV, Bochvar NR, Janecek M (2014) Effect of deformation schedules and initial states on structure and properties of Cu-0.18 % Zr alloy after high-pressure torsion and heating. Mater Sci Eng A. 598:288–292
22. Ribárik G, Gubicza J, Ungár T (2004) Correlation between strength and microstructure of ball-milled Al–Mg alloys determined by X-ray diffraction. Mater Sci Eng A. 387–389:343–347
23. Balogh L, Ribárik G, Ungár T (2006) Stacking faults and twin boundaries in fcc crystals determined by X-ray diffraction profile analysis. J Appl Phys. 100:023512
24. Gubicza J, Dobatkin SV, Khosravi E, Kuznetsov AA, Lábár JL (2011) Microstructural stability of Cu processed by different routes of severe plastic deformation. Mater Sci Eng A. 528:1828–1832